CHARLES UNIVERSITY

Faculty of Pharmacy in Hradec Králové

Department of Pharmaceutical Technology

Factors affecting the microstructure and permeability of lipid model membranes

Diploma thesis

Omran Zamani Gerashi

Hradec Králové 2024

Supervisor: Dr. Georgios Paraskevopoulos, Ph.D.

Consultant: Dr. Irene Sagrafena

I hereby confirm that this thesis is my original copyrighted work. I compiled and elaborated it independently in my own words and in accordance with copyright. All resources and literature I used are indexed in the bibliography and properly cited. The thesis was not written and intended as misuse for obtaining the same or different academic degree.

In Hradec Králové 2024 Omran Zamani Gerashi

Acknowledgments

I'd like to firstly thank Dr. Georgios Paraskevopoulos Ph.D. for accepting me to complete my thesis under the prestigious skin barrier research group. With each challenge I faced during this time, I received exceptional support from the team. I would like to also highlight the tremendous help I received from my consultant, Dr. Irene Sagrafena, I am very grateful for the opportunity.

To my family I am indebted for all their support throughout this degree, I couldn't have gotten this far without them. I am also endlessly grateful for the lifelong friendship I built there in Hradec Kralove.

Finally, I'd like to express sincere appreciation to the Charles University (GAUK 1156120, SVV 260 661) and the Czech Science Foundation (GACR number No. 22-20839K) for funding this project and making this research possible.

Abstrakt

Univerzita Karlova, Farmaceutická fakulta v Hradci Králové

Katedra Farmaceutické technologie

Školitel: Dr. Georgios Paraskevopoulos, Ph.D.

Konzultant: Dr. Irene Sagrafena

Autor: Omran Zamani Gerashi

Název diplomové práce: Faktory ovlivňující mikrostrukturu a propustnost membrán lipidového modelu

Stratum corneum (SC), svrchní vrstva epidermis, je rozhodující pro udržení bariérové funkce kůže. Architektura SC je důležitým faktorem při regulaci vlhkosti pokožky. Volná voda (H_2O) může difundovat z pokožky do okolního prostředí, zatímco vázaná H_2O je spojována s řadou molekul, definovaných jako přirozené zvlhčující faktory (NMF). Tato směs sloučenin zahrnuje aminokyseliny, kyselinu mléčnou, kyselinu pyrrolidonkarboxylovou, glycerol, močovinu a minerální ionty.

Cílem této studie bylo prozkoumat potenciální účinky složek NMF na mikrostrukturu a permeabilitu lipidů v modelových lipidových membránách napodobujících SC. Vybranými NMF byly kyselina pyrrolidonkarboxylová, kyselina urokanová, glycerol a močovina s cílem určit, zda jejich přítomnost může ovlivnit jak lamelární, tak laterální organizaci lipidických směsí. Experiment ukázal, že zkoumané NMF nebyly schopny zadržovat H_2O při laboratorní vlhkosti po delší dobu. Jako nejúčinnější NMF byl stanoven glycerol, protože lipidové membrány obsahující glycerol dokázaly absorbovat maximální množství H_2O a zároveň ji nejméně ztrácet.

Abstract

Charles University, Faculty of Pharmacy in Hradec Králové

Department of Pharmaceutical Technology

Supervisor: Dr. Georgios Paraskevopoulos, Ph.D.

Consultant: Dr. Irene Sagrafena

Author: Omran Zamani Gerashi

Title of the thesis: Factors affecting the microstructure and permeability of lipid model membranes

The stratum corneum (SC), the epidermis' outermost layer, is critical for maintaining skin barrier function. The architecture of the SC is an important factor in skin moisture regulation. Free water (H_2O) can diffuse from the skin into the surrounding environment, whereas bound H_2O is associated with a variety of molecules, defined as natural moisturizing factors (NMF). This mixture of compounds includes amino acids, lactic acid, pyrrolidone carboxylic acid, glycerol, urea, and mineral ions.

The aim of this study was to investigate the potential effects of NMF components on lipid microstructure and permeability in model lipid membranes. The NMF chosen were pyrrolidone carboxylic acid, urocanic acid, glycerol, and urea with the goal of determining whether their presence can affect both lamellar and lateral organization of lipidic mixtures. The experiment showed that the NMF investigated were incapable of retaining H_2O at ambient humidity for an extended period. Furthermore, glycerol was the most effective NMF because glycerol containing lipidic membranes proved to absorb the maximum amount of H_2O and lose the least.

Table of contents

List of tables and figures

1. List of abbreviations

Cer	Ceramides
Cer [EOS]	N-(30-linoleoyloxy-triacontanoyl)-sphingosine
Chol	Cholesterol
EI	Electrical impedance
EtOH	Ethanol
FFA	Free fatty acids
FTIR	Fourier-transform infrared spectroscopy
Gly	Glycerol
H_2O	Water
His-rich	Histidine-rich
HPLC	High performance liquid chromatography
IND	Indomethacin
LPP	Long periodicity phase
NMF	Natural moisturizing factor
PBS	Phosphate buffered saline
PCA	Pyrrolidone carboxylic acid
PG	Propylene glycol
SPP	Short periodicity phase
SC	Stratum corneum
TH	Theophylline
TEWL	Trans epidermal water loss
UV	Ultraviolet
UCA	Urocanic acid

XRD	X-ray diffraction

2. Introduction and Aim of the work

The skin is the most extensive organ of the integumentary system, covering the entire body. The hypodermis, dermis, and epidermis are the three layers of the skin. The Stratum Corneum (SC) is the epidermis outermost layer and is essential for maintaining the skin barrier [1]. The architecture of the SC is a critical factor in skin moisturization. SC damage reduces the skin's ability to retain H_2O, causing drying and impairing the barrier function. Free H_2O can diffuse from the skin to the surrounding environment, whereas bound H_2O is associated with many molecules such as filaggrin, natural moisturizing factor (NMF) including amino acids, lactic acid, pyrrolidone carboxylic acid (PCA), glycerol (Gly), urea, and mineral ions [2, 3].

The skin lipid membrane model elucidates the intricate arrangement and function of lipids within the SC which are crucial for hydration maintenance and barrier function [4].

Lipid model membranes serve a variety of purposes across different fields of science, due to their ability to simulate essential aspects of biological membranes in a controlled environment. They are widely used in biophysical research to investigate fundamental membrane properties such as lateral organization, phase transitions, membrane fluidity, and lipid-lipid interactions. The main factors affecting the permeability and microstructure of lipid model membranes, providing an explanation for further study [5]. This includes the different lipid species, their compositional differences, and the influence of lipid chemistry on membrane properties. Different aspects such as pH, temperature, and the presence of additives can modulate these membranes' structure and alter permeability properties [6, 7].

This study aims to gain insight into the potential effects of NMF components on lipid microstructure and permeability in model lipid membranes. PCA, UCA, Gly, and Urea were chosen as NMFs for this study. To see if the presence of NMFs affected the lamellar and lateral structures of lipidic mixtures, Confocal Raman microspectroscopy, Fourier-transform infrared spectroscopy (FTIR), and X-ray diffraction (XRD) were used. To demonstrate how different molar ratios of NMF affected lamellar lipid organization, throughout the experiment different NMF molar ratios were used, specifically 50%, 10%, and 5%. This study further investigated NMFs' ability to absorb and retain H_2O using a H_2O loading experiment and dehydration kinetics.

3. Theoretical part

3.1. Skin

Being the most extensive organ of the integumentary system, the skin is covering the entire human body. Following an inside out direction, hypodermis, dermis, and epidermis are the layers that comprise the skin. (Figure 1). Skin is the initial defense against chemicals, infections, UV rays, and physical damage. It is also controlling the body temperature and the quantity of H_2O escaping into the environment [1].

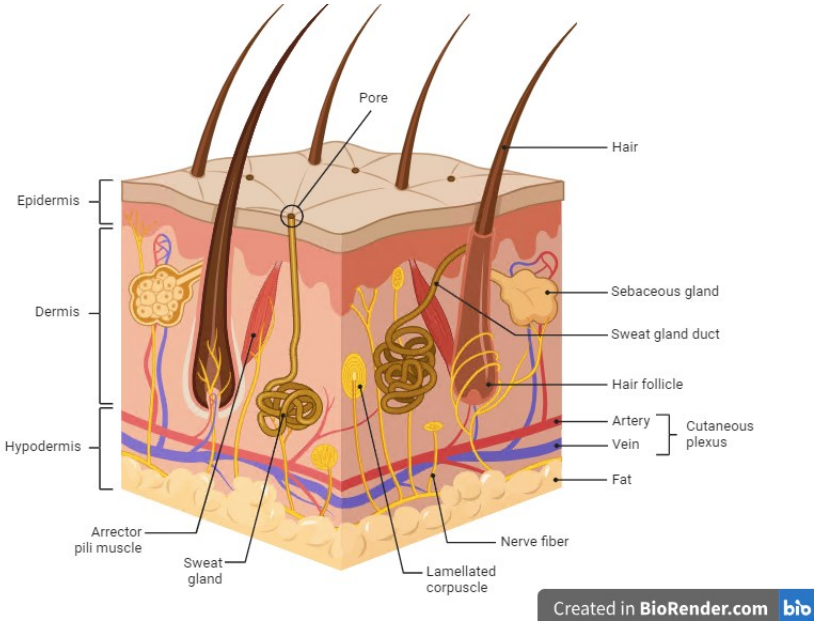

Figure 1. Anatomy of human skin

3.1.1. Hypodermis

The hypodermis is the layer under the dermis. It joins the fibrous tissue of the muscles and bones to the skin The hypodermis consists of adipose tissue (responsible for insulation and working as a fat reservoir) and areolar connective tissue (loose and well-vascularized tissue). The hypodermis is additionally referred to as the subcutaneous layer or the superficial fascia [8].

3.1.2. Dermis

The middle layer of the skin that provides mechanical strength is called dermis. The membrane which separates the dermis from the epidermis is called the basal membrane. Blood vessels, hair follicles, lymphatics, nerves, and sweat glands are the main components of the dermis. This layer's vascular network provides nutritional support to tissues and maintains homeostasis [1]. The lymphatic vasculature in this layer consists of pre-collector vessels that drain lymph fluid into subcutaneous lymphatics and primary lymphatics that absorb fluid from the interstitium [9, 10]. The lymphatic vasculature is in charge of immune response, tissue fluid homeostasis, and dietary fat absorption. It also plays a vital part in a variety of diseases, including cancer, chronic inflammation, and lymphedema [11-14]. The two structurally distinct layers of dermis are the papillary layer, which is closer to the surface of the skin and the reticular layer, that is separated from the papillary via a vascular plexus [15]. In traditional transdermal delivery, drugs must pass via the epidermis' SC before reaching the capillaries of the papillary dermis. These blood vessels are the path of applied drugs to reach the circulatory system, while the remaining drug in the papillary dermis might penetrate more profound into the reticular dermis. Transdermal delivery is a great drug delivery method because of enabling continuous drug administration without repeated invasive procedures [16, 17].

3.1.3. Epidermis

The epidermis is the protector of skin against environmental hazards by acting as a chemical, physical, as well as biochemical barrier [18]. The five main layers of the epidermis are the following: stratum basale, stratum spinosum, stratum granulosum, stratum lucidum, and SC. Stratum basale is the epidermis' deepest layer containing cube- and column-like stem cells which are mitotically active and are continuously producing keratinocytes. Melanocytes are also present in this layer. In the stratum spinosum are found non-typical polyhedral cells which are involved in cytoplasmic processes and connected via desmosomes. This layer also contains dendritic cells. The stratum granulosum consists of cells with bundles of keratohyalin granules and lamellar granules containing glycolipids. The stratum lucidum is a very thin layer of dead skin cells [19]. Lastly, the SC is the outermost layer of epidermis and where the cells are in the last stage of keratinocyte maturation and development. The SC of the human body is composed of around 15 layers of compressed corneocytes separated into the stratum compactum and the stratum disjunctum [20]. A separate chapter will be dedicated to the SC.

3.2 Stratum corneum

The SC is the most crucial epidermis layer in the maintenance of the skin barrier. The SC acts as an obstacle between the environment and the skin's deeper layers, blocking toxic substances from entering the body and preventing skin dehydration (Figure 2) [20].

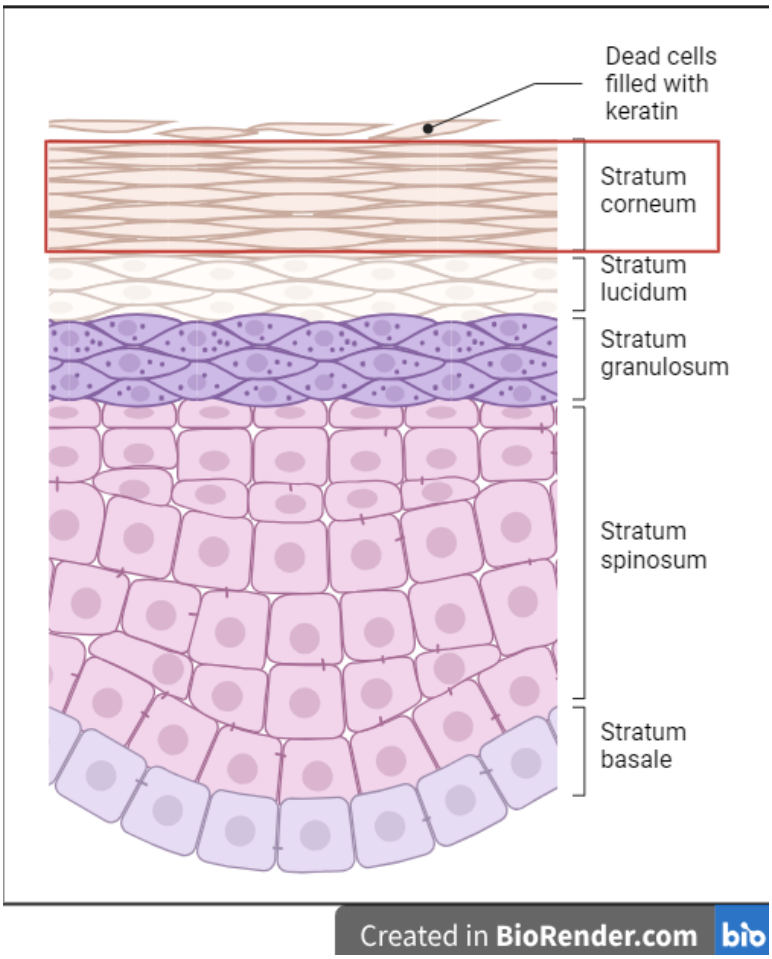

Figure 2. Stratum corneum.

The SC's main components are corneocytes, which are flattened dead keratinocytes at the last stage of differentiation filled with keratin and covered by a lipid layer that is parallelly aligned to the surface of the cell (known as corneocyte lipid envelope) [21]. The space between the corneocytes is filled by the lipidic matrix. SC lipids represent ~20% of the SC volume [22]. Cholesterol (Chol), free fatty acids (FFA), and Ceramides (Cer) are the three major classes of lipids that constitute this matrix (Figure 3). These major physiological SC lipids are synthesized within the SC enzymatically from specific lipid precursors [23-26].

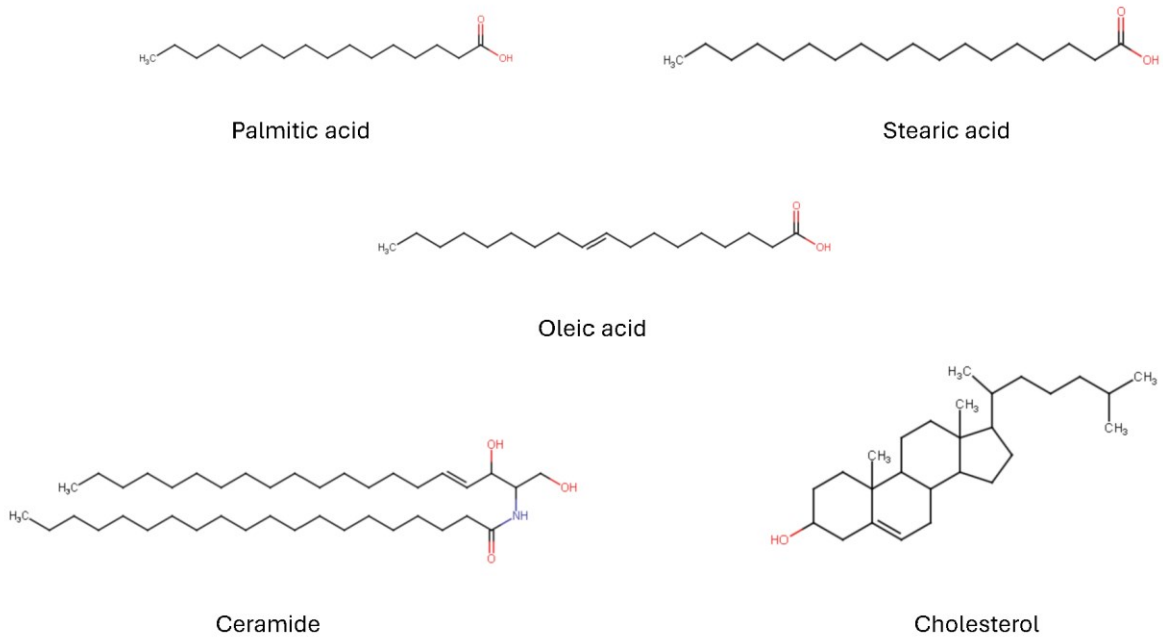

Figure 3. Chemical structures of Cer, FFA and Chol. Structures created by ChemAxon.

SC lipids can coexist within different lamellar phase organizations known as the short periodicity phase (SPP) and the long periodicity phase (LPP). SPP and LPP have a repeated distance of ~5-6 nm and ~13 nm respectively. The LPP plays a crucial role in the optimal barrier properties and is uniquely connected to the human skin barrier. [27-29]. Furthermore, exists another degree of organization within the lipid matrix, known as lateral packing, which is important for skin permeability. While a smaller lipid pool forms a hexagonal or liquid phase which are packed less densely, the majority of the them are packed in an orthorhombic structure [30]. The skin's barrier function relies heavily on both lateral and lamellar lipid organization (Figure 4) [31-33]. However, the lack of proper lamellar alignment has been demonstrated to affect more the skin barrier function than the lateral packing change from orthorhombic to hexagonal [34].

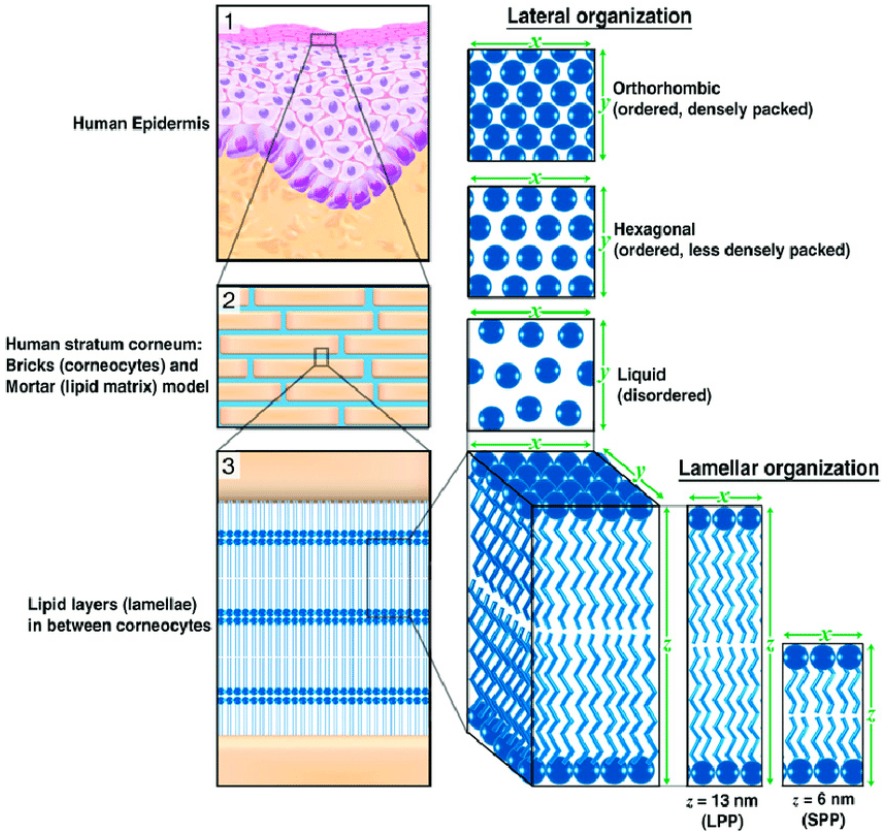

Figure 4. Lamellar and lateral packing of the skin. Adapted from Janssens et al [35]

In the central region of the LPP, there are C24 acyl chain Cer (without hydroxy functionalization) linked to sphingosine moiety with 18 carbons (NS) while the outer region mainly consists of Chol [36]. Omega-O-acyl Cer, (i.e. 32-linoleoyloxydotriacontanoyl sphingosine (Cer [EOS])) are an important part of the skin barrier, which are limiting the excessive water loss and the undesirable substances to go through the skin [37]. Cer[EOS] can be found within the inner parts and also outer parts of LPP. The headgroups are located at approximately the edge of each unit cell while the aliphatic chain extends close to the center of the headgroup, where the linoleate fragment is located [27]. As previously mentioned, the SC lipid matrix contains Chol which also plays a crucial role in the organization of lipids in SC. In fact when Cer [EOS] is not present, only SPP is formed, whereas when Chol is absent neither SPP nor LPP is formed [38, 39].

Alterations at the lipid composition within the SC lipid mixture have related to pathological conditions. For example, inflammatory skin diseases (eg psoriasis and seborrheic or atopic dermatitis) exhibit an alteration at the level of the lipidic matrix, with increased levels of FFA which contributes to impaired skin barrier function [40-44]. Furthermore, barrier dysfunction can be caused by changes in Cer subclasses ratio [45]. The lipid content of the SC

is not only having an influence on the proper skin barrier function, but also on the content of H_2O. The architecture of the SC is a critical factor in skin moisturization. SC damage reduces the skin's ability to retain H_2O, causing drying and impairing the barrier function. Free H_2O can diffuse from the skin to the surrounding environment, whereas bound H_2O is associated with many molecules such as filaggrin, NMF including amino acids, lactic acid, PCA, Gly, urea, and mineral ions [2, 3].

3.3 Natural moisturizing factor

NMF is a mixture of water-soluble, hygroscopic, low molecular weight, compounds that are produced by the breakdown of filaggrin, a histidine-rich (His-rich) protein, in keratinocytes. They constitute for 10% of corneocytes and 20% of the SC dry weight [46, 47]. Profilaggrin (> 500 kDa) is a protein with high phosphorylation found in the epidermis (keratohyalin granules). It is composed of 10-12 multiple filaggrin connected by a short hydrophobic peptide linker. Profilaggrin is dephosphorylated when mature granular cells are changing to corneocytes, resulting in filaggrin (37 kDa). Filaggrin His-rich is a transient component that only exists in the upper 2 to 3 layers of SC. NMF is produced by its complete proteolysis (Figure 5).

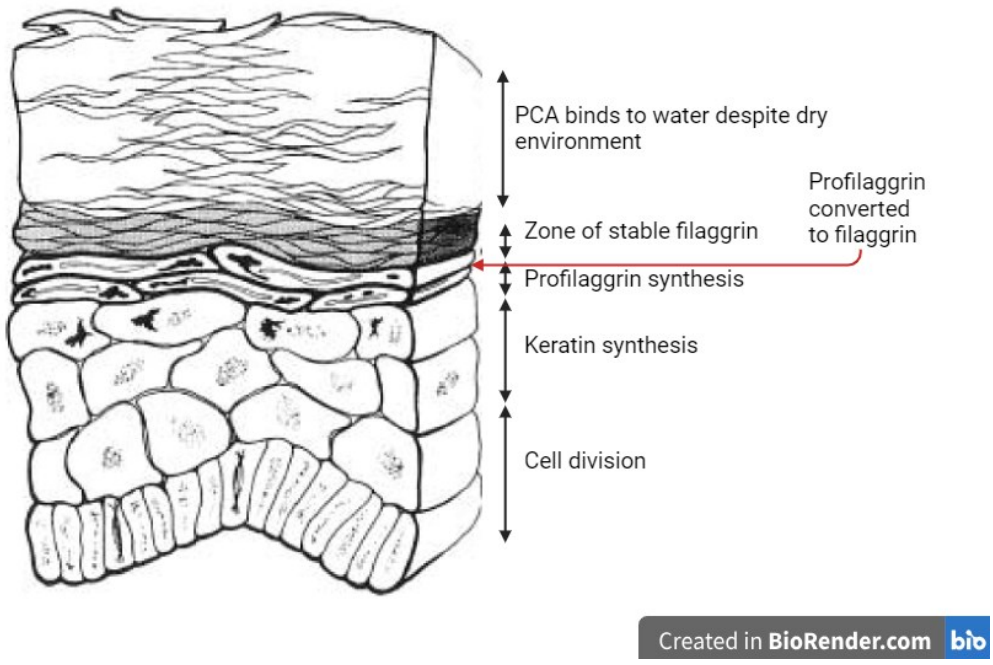

Figure 5 . Conversion of Profilaggrin to Filaggrin.

The NMF is mainly made up of non-bounded amino acids and their derivatives, including inorganic salts, PCA, UCA along with urea, lactic acid and sugars (Table 1) [48, 49].

Table 1: Chemical composition of NMF, adapted from Ref. [2]

Chemical	Composition %
Free amino acids	40
Lactate	12
PCA	12
Sugars	8.5
Chloride	6
Urea	7
Potassium	4
Sodium	5
Calcium	1.5
Ammonia, uric acid, glucosamine, creatine	1.5
Magnesium	1.5
Phosphate	0.5

The NMF's function is to keep the skin hydrated. The proper SC hydration has four important functions: protecting and maintaining skin plasticity, enabling hydrolytic enzymes to function (desquamation process), maintaining the acidic mantle of the skin (specific to UCA), and contributing to the SC's optimal barrier function. NMF are hygroscopic in nature, acting as humectants by absorbing atmospheric H_2O, enabling the outermost SC layers staying hydrated despite the external environment's desiccating action [2, 50].

The H_2O gradient within the SC has been identified as the indicator which initiates protein lysis at a particular point of the maturation of SC. The release of the NMF components occurs only after the corneocytes are compressed and moved to drier regions of the SC and the cornified envelope has reinforced. During the last stage of differentiation of keratinocytes, the

cornified envelope forms below the cell membrane. It is extremely strong and highly insoluble. [51]. Some free amino acids remain in the SC layers once they are released. At the same time, a smaller pool is converted into their derivatives (for example PCA and UCA) via enzymatic and non-enzymatic reactions. PCA is produced by non-enzymatic hydrolysis of glutamine, whereas UCA is produced by a deaminase reaction from histidine [48, 52-54].

Gly is extracellular to corneocytes and continuously absorbs H_2O when the relative humidity is high. The SC components are significantly stiffer at moderate relative humidity, when these substances are absent. This substance also increases the mobility of proteins and lipids which are present in the SC [55].

PCA is the most abundant type of NMF in the SC, that's why it is used as a general indicator of total NMF content. It is highly hygroscopic and can absorb H_2O at 92% relative humidity and having little impact on molecular mobility [2, 55].

UCA is the major chromophore of the skin, making up to 0.5% of the dry weight of the epidermis. It exists both in the cis- and its more stable trans- forms, which, upon absorption of UV radiation, it is converted to the cis- isomer, the one exerting an immunoregulatory role. It is less polar than other NMF and is responsible for the maintenance of the SC's acidic mantle, as well as influencing the mobility of the SC's lipid regions.[50, 55-57].

When the SC components are significantly stiffer at moderate relative humidity in the absence of these compounds, urea is an extracellular solid that increases the mobility of the proteins and lipids. [55].

3.4 *In Vitro* model lipid membranes

Drug percutaneous permeation testing has been used as an important way of evaluating (trans)dermal delivery systems. The in vivo human setting is the best way to carry out the evaluation [58]. Apart from excised human skin, several models of animal skin, including those from reptiles, rodents, and mammals, have been previously used as substituents of the human skin [59-65].

Since using human or animal skin can be complicated due to ethical, practical, or economic reasons, variety of models, including animal models and ex vivo human skin models, and reconstructed or artificial skin models, have been developed [58]. Lipid model membranes are one of these models that are used in skin research for a variety of reasons. Firstly, real skin samples vary in composition, and different donors have different lipid compositions, which may affect data reproducibility [66]. Furthermore, human skin experiments require prior ethical approval, which is not always readily available. Additionally, human skin has more variable characteristics than the skin from other species, such as pigs or guinea pigs, with respect to permeability [67]. Thus, in vitro lipid membranes are used as skin substitute for permeation studies [68]. Plenty of artificial models have been created to replicate the intact barrier properties of healthy skin. So far, a couple of them have the potential to closely resemble the compromised skin. In vitro models containing synthetic or tissue-extracted SC lipids have been considered as a valuable tool to study the effect of different Cer composition on the drug permeation [69-74].

3.5 Techniques used for analyses

3.5.1 HPLC

As one of the most useful techniques, high performance liquid chromatography (HPLC) has been previously used for separating, characterizing, and analyzing biological, clinical, and pharmaceutical samples. In recent years, HPLC has been used to develop targeted separation methods for analyzing targets such as disease biomarkers, drugs, and biopharmaceuticals [75]. HPLC, which works on the principle of liquid chromatography, involves the passage of a sample together with a suitable mobile phase through a stationary phase filled column. The elution of the sample's components through the column depends on their interactions with the column material (stationary phase), inducing their distinct retention times [76]. The HPLC technique includes preparation of the sample, injecting it into the column, monitoring the separation, and analyzing the results (Figure 6) [77]. HPLC's versatility is demonstrated by various methods, including normal and reverse phase HPLC, which cater to different separation requirements [78]. In normal phase HPLC can be found the combination of a polar stationary phase with a nonpolar mobile phase, allowing the separation of polar compounds [79]. In contrast, reverse phase HPLC combines a nonpolar stationary phase with a polar mobile phase, making it more effective for the separation of hydrophobic compounds [76]. In HPLC, the properties of the stationary and mobile phases have a significant impact on separation efficiency. The mobile phase (one solvent or a mixture of different solvents) is selected based on its compatibility with the analytes and stationary phase. In normal-phase HPLC nonpolar solvents (such as hexane) are commonly used as mobile phase, whereas in reverse phase HPLC polar solvents (such as H_2O and acetonitrile) are commonly used [79]. The stationary phase, on the other hand, interacts directly with the sample's components through a variety of basic modes of interaction related to affinity, size, and electrostatics. [80].

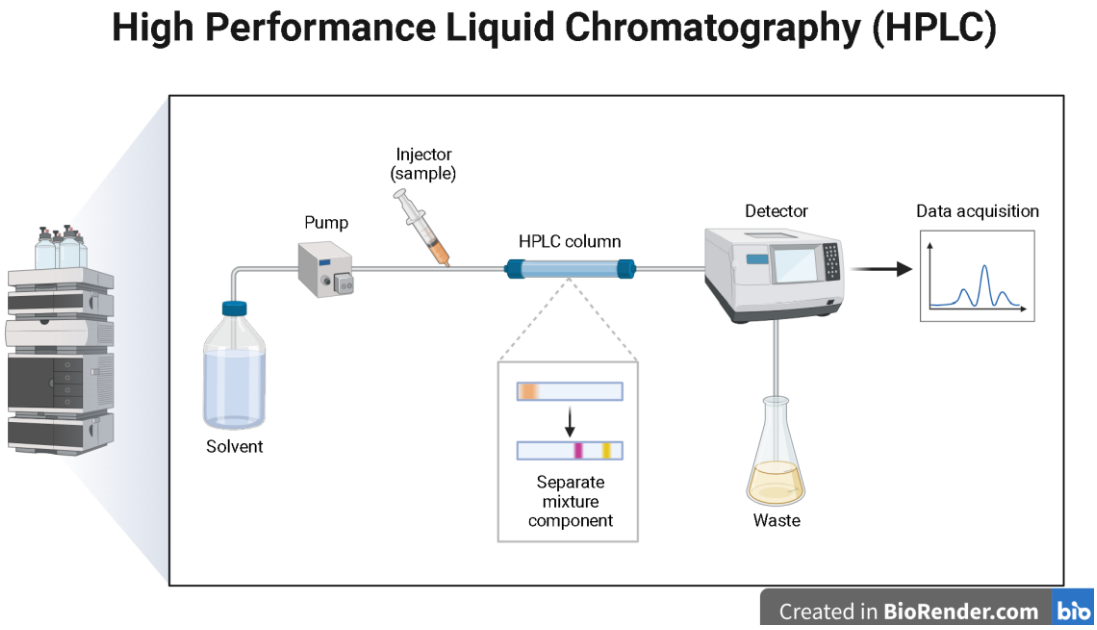

Figure 6. HPLC system explained.

3.5.2 Raman Spectroscopy

The evaluation of skin structure has become possible with optical imaging techniques such as confocal microscopy. However, identifying individual skin components using the abovementioned optical methods remains difficult because of complexity of the tissue, morphological differences are observed using the refractive index at the cell boundary [81]. Imaging systems contribute to the development of topical drugs as well as the diagnosis, evaluating, and classifying multiple diseases in the skin. Raman spectrometry, a non-destructive vibration spectroscopy, is widely used for a variety of structural analysis techniques which uses the excitation of vibrational energy transitions. This method is appropriate to produce chemical maps. Raman spectroscopy plays an important role in driving new technological developments with using of optical effects that accurately reflect the structure and chemical properties of the molecules in the samples, allowing for accurate observation of chemical reactions in living cells and tissues. Being an optical technique which is relying on the non-elastic scattering of light, Raman spectroscopy can be described as the scattering result of a light beam when it strikes a particle. During this strike, most of the light is elastically scattered, and a portion of the beam passes through. When photons in a beam interact with molecular vibrations in a sample, their energy changes, causing electrons in a molecule's bond to be distorted. The radiation is reemitted when the system returns to normal (Figure 7) [82, 83]. Raman spectroscopy analyzes the skin, modifications of the skin composition which might

be caused by maturity or chronic conditions and analysis of drug delivery to the skin which are typically performed by obtaining spectra along a line perpendicular to the skin surface or by 2D imaging [84].

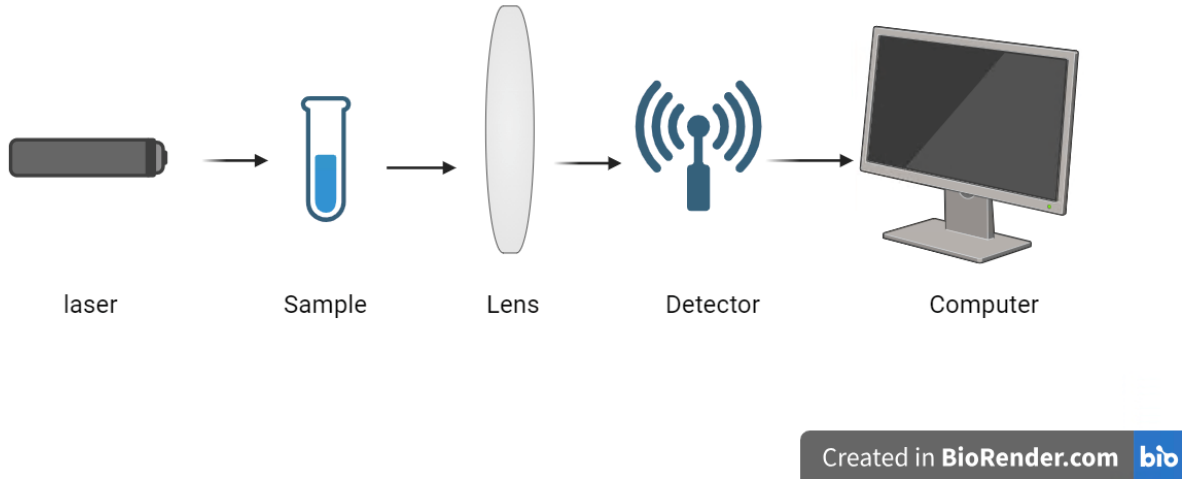

Figure 7. Principle of Raman spectroscopy.

3.5.3 Trans epidermal water loss (TEWL)

TEWL is a characteristic of skin tissue that rises when the barrier properties are damaged. Thus, TEWL measurements are used as an indicator of skin barrier integrity. The term TEWL refers to the H_2O flux density that penetrates the tissue's surface from the SC through the dermis and the lower layers of epidermis [85, 86]. It has been defined in guidelines as a common tool to measure wide range of skin and dermatological research studies [87, 88]. Although the observation of TEWL is not direct, TEWL can be evaluated using devices that have temperature and humidity sensors which analyze the skin's H_2O evaporation density gradient [86]. They are also linked to a leading technology program, which produces high quality results. TEWL measurement devices come in closed, open and semi-open chamber systems [86]. To measure TEWL, a probe is applied to the surface of the skin. This probe detects shifts in the local humidity that exceed ambient humidity values, allowing it to track H_2O vapor density changes over time above a specific skin area (Figure 8) [89, 90].

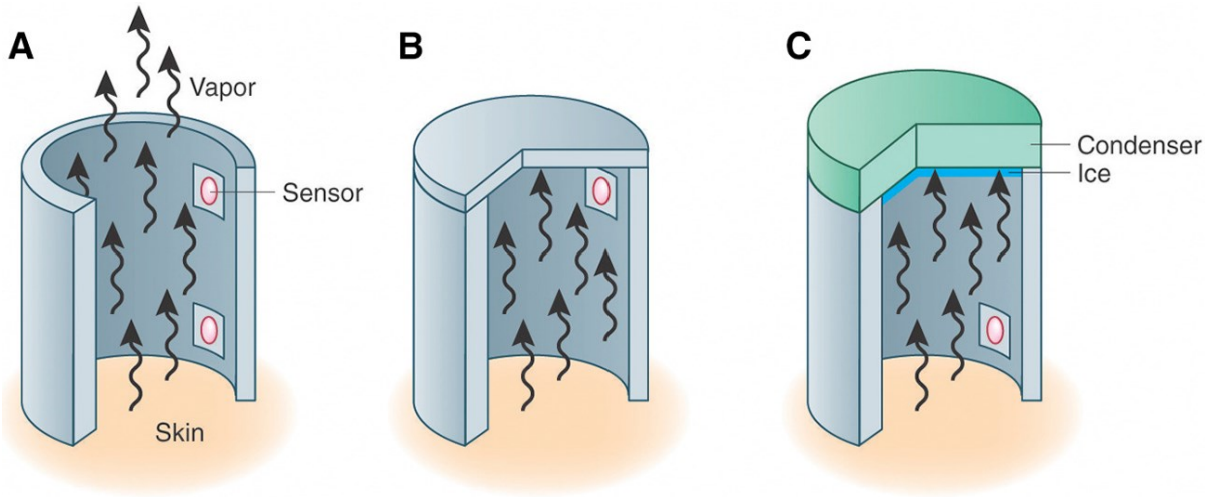

Figure 8. TEWL device. Adopted from Alexander et al [91]

3.5.4. Electrical impedance (EI)

EI is a common method for evaluating skin integrity in a non-invasive and rapid method. A circuit with a resistor and capacitor connected in parallel is an analogous model of skin impedance [92]. EI measurements is an effective way to characterize the integrity of a wide range of tissues, including human and animal skin. This technique comprises on the application of a small-amplitude sinusoidal modulation to an input current (or potential). Subsequently, a measurement of the new resulting current (or potential) is taking place. The skin's direct current resistance is determined by the SC's resistivity and thickness. Also the resistance of the skin is inversely related to the ability of ions or polar substances to permeate through it (Figure 9) [93].

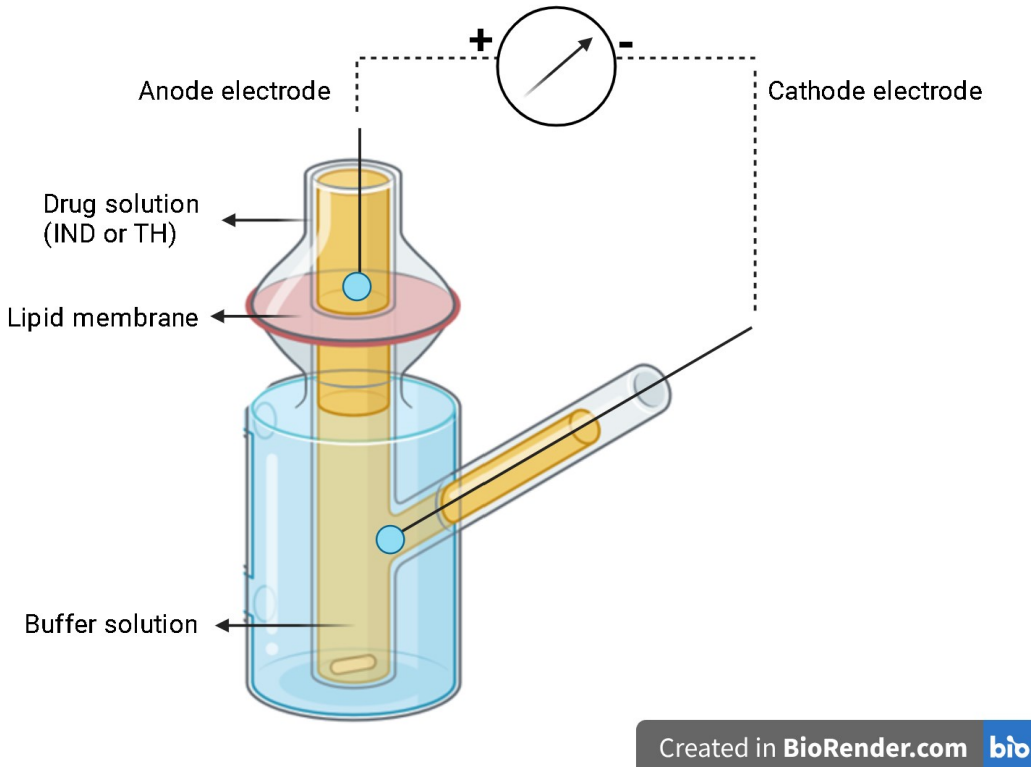

Figure 9. Electrical impedance measurement performed in this study.

4.Experimental part

4.1. Materials and methods

4.1.1 Materials

2-pyrrolidone-5-carboxylic acid (PCA), Glycerol (Gly), indomethacin (IND), theophylline (TH) and propylene glycol (PG) were acquired from Merck (Darmstadt, Germany). Trans urocanic acid (UCA) was purchased from TCI (Tokyo, Japan). Ethanol 96% (EtOH) and hexane both of pro analysis quality were purchased from Penta ((Hostivař, Czech Republic). Millipore H_2O cleaned through a Millipore Q purification system (Merck Millipore, Burlington, Massachusetts, USA) was employed to prepare aqueous solutions. Lipid mixtures were sprayed on 22 x 22 mm^2 Esco cover glasses for microscope (Erie Scientific, Portsmouth, NH, USA).

4.1.2 Methods

4.1.2.1. Sample preparation

Previously purified and analyzed human skin lipids with an equal molar ratio of Chol, Cer and FFA were used for the needs of this study.

Solutions of lipids were prepared at a concentration of 1.25 mg/mL by dissolving the lipids in hexane: EtOH 96% (2:1 v/v).

NMF stock solutions with a concentration of 1 mg/mL were prepared after dissolving appropriate amounts of PCA or UCA in EtOH 96%; or urea in hexane: EtOH 96% (2:1 v/v). Gly stock solution was prepared by mixing it with EtOH 96%.

To homogenize the samples, a Genie-2 vortex device (Scientific industries, Bohemia, NY, USA) and an ultrasonic water bath sonicator Kraintek 12 (Kraintek Czech, Hradec Kralove, Czech Republic) were used.

Appropriate amounts of NMF solutions were added to the lipid solutions to follow the conditions described in Table 2. Control samples included only the lipidic mixture in absence of NMF.

Table 2. Investigated molar% in the experiment.

	Lipids(mg)	NMFs molar ratio (%)
control	0.25	+ 0%
A	0.25	+ 50%
B	0.25	+ 10%
C	0.25	+ 5%

Following the addition of the desired amount of NMF to the lipids, all solutions were homogenized, vortexed and sonicated.

4.1.2.2. Spraying of the samples

A Linomat V instrument from Camag (Muttenz, Switzerland) with additional y-axis movement was used for the spraying under a continuous nitrogen stream (10.2 µL/min) on different surfaces. For the biophysical experiments the lipids were sprayed on 22 x 22 mm^2 Esco cover glasses for microscope (Erie Scientific, Portsmouth, NH, USA)- (2x100 µl per 1 cm^2). For the permeability experiments the lipids were sprayed on 0.015 µm pore size polycarbonate filters from Whatman (Maidstone, Great Britain) - (2x 100 µl per 1 cm^2).

4.1.2.3. Desiccation

Following spraying, the samples were placed in the desiccator (containing phosphorous pentoxide and paraffin) and left there under vacuum overnight.

4.1.2.4. Annealing

The next day, samples were removed from the desiccator, and were prepared for annealing. The mass of the lipids which were sprayed on the glass support was measured before annealing.

Samples were placed in an aluminum annealing container with their lipids facing up, supported by circular aluminum supports 2 ml of Millipore H_2O were added precisely beneath the samples and the annealing container was sealed. The samples were heated in an oven (Memmert, Schwabach, Germany) at 70 °C for 20 minutes and subsequently allowed to slowly cool down for 4 hours until room temperature was reached.

4.1.2.5. Water loading

After the 4 hours of the cooling down of the annealing step, samples were weighted on the analytical balance to determine the amount of H_2O loaded during the annealing step.

4.1.2.6. Kinetic of dehydration

As soon as the H_2O loading value was obtained, without moving the sample, the kinetic of dehydration detection process began after 10 minutes. A measurement was taken every 10 minutes for up to 1 hour, and then every 20 minutes for up to 3 hours.

4.1.2.7. X-ray diffraction

XRD studies of the model lipid membranes were carried out on an X'Pert PRO $\theta - \theta$ powder diffractometer from PANalytical B.V. (Almelo, Netherlands) at room temperature, humidity, and atmospheric pressure. The instrument was using Para focusing Bragg-Brentano geometry and Co Kα radiation (λ = 0.17903 nm, U=35 kV, I=40 mA) in customized sample holders over an angular range of 0.6−30° (2θ). An ultrafast position-sensitive linear, one-dimensional (1D) X'Celerator detector with a step size of 0.0167° (2θ) and a counting time of 20.32 s $step^{-1}$ was used to scan the data. The data was assessed with X'Pert Data Viewer software from PANalytical B.V. (Almelo, Netherlands).

4.1.2.8. Fourier-transform infrared spectroscopy (FTIR)

Infrared spectra were measured on a Nicolet 6700 spectrometer (ThermoScientific, Waltham, MA, USA) outfitted via single-reflection MIRacle ATR Germanium crystal (PIKE Technologies, Fitchburg, WI). During the measurements, a constant pressure clamping mechanism was employed.

The spectra were measured by combining 256 scans at a resolution of 2 cm^{-1} at room temperature.

4.1.2.9. Confocal Raman microspectroscopy

Raman spectra and optical images were collected at room temperature using a confocal Raman microspectrometer WITec Alpha 300R (WITec Wissenschaftliche Instrumente und Technologie GmbH, Ulm, Germany). The excitation radiation wavelength of a diode/solid-state laser was 633 nm. A spectrograph UHTS 300 connected with a thermoelectrically cooled charge-coupled device detector was used for the collection of spectra. Objectives (Zeiss) EC „Epiplan“DIC with 10× magnification, EC Epiplan-Neofluar“ DIC with 100× magnification, and a diffraction gratin 600 lines/mm were used. Experimental data were evaluated using WITec Project FIVE+ software.

4.2 Permeation experiment

For the permeation experiment, a total of 38 samples were prepared. (8 PCA, 7 UCA, 8 Urea, 8 Gly, 7 control) (Table 3).

Table 3. Preparation of samples.

Sample name	Mol% lipids	Mol% NMF
Control	100	0
PCA-5	95	5
UCA-5	95	5
Urea-5	95	5
Gly-5	95	5

4.2.1 Preparation of model membranes for permeation

Samples were prepared following what was previously described in section (4.1.2). The model lipid membranes were encased between Teflon holders with a diffusion area of 0.5 cm^2 and assembled in Franz diffusion cells (Figure 10). Phosphate-buffered saline (PBS) (pH 7.4) containing 50 mg/L gentamicin was used as acceptor phase for the permeation experiments.

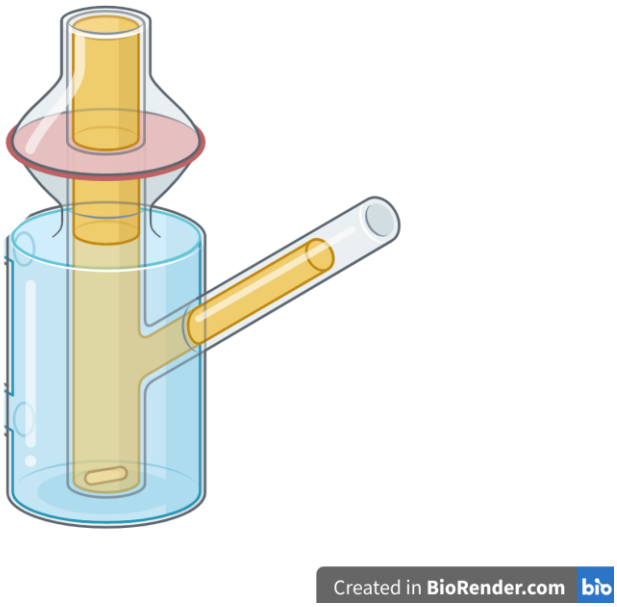

Figure 10. *Diffusion Franz cell*

PBS was prepared as described by Table 4 and the pH was adjusted with a small amount of concentrated aqueous solution of sodium hydroxide (NaOH) to reach the value of 7.4

Table 4. Preparation PBS buffer pH 7.4

PBS pH 7.4	
$NaH_2PO_4 * 2H_2O$	0.624 g
$Na_2HPO_4 * 12H_2O$	5.730 g
NaCl	16 g
KCl	0.403 g
Gentamycin	0.1 g
Millipore H_2O	2 L

The precise volume of each acceptor phase was measured, and the obtained value was later included in the calculation of the flux values. A magnetic rod was added in the acceptor phase to ensure constant stirring throughout the experiment.

The Franz diffusion cells were placed in a temperature-controlled water bath (32°C) and were equilibrated for 12 hours. TEWL and EI were measured following equilibration period.

4.2.2 Trans Epidermal Water Loss (TEWL)

An Aquaflux AF200 (Biox Systems Ltd, London, England) equipped with temperature and RH sensors was used to measure the H_2O loss through model films. Each Franz cell was taken out of the water bath, its top half was taken off, and the probe was placed on the Teflon holder. Aquaflux Software Version 9.3 was used to record the value of the average steady-state. Each sample was measured twice, and the average of these two values was used.

4.2.3. Electrical impedance (EI)

An LCR meter 4080 from Conrad Electronic (Hirschau, Germany) was used to measure electrical impedance. Each Franz-type diffusion cell filled with 500 µL of PBS (pH 7.4) and equilibrated for 1 hour. The impedance of the lipid membrane was measured by submerging each of the probe tips in the buffer of the donor and the acceptor chambers of the Franz diffusion cell. Each measurement was performed twice and the average of these two values was used. The PBS was removed from the donor compartment after the EI measurements.

4.2.4. Permeation of model compounds

Following the TEWL and EI measurements, 100 µL of 5% TH suspension in 60% PG in H_2O were applied to the donor chamber of each model membrane. The used formulation provided sink conditions for the investigated model compound. After the application, every 2 hours for 10 hours, samples (300 µL) were taken out from the acceptor phase and replaced with the same volume of PBS. Following the initial 10-hour permeation experiment, the formulation left-overs were gently rinsed away with PBS and the remaining PBS was removed (cotton swabs). The lipid membranes were further equilibrated for 12 hours. Following that, 100 µL of the second formulation (2% suspension of IND in 60% PG in H_2O) were applied. The IND permeation experiment was performed similarly as described earlier for TH.

4.2.5. Preparation of HPLC mobile phases for the two permeants

For the preparation of TH mobile phase, 18.7 g of NaH_2PO_4 *$2H_2O$ was added to 1200 mL of Millipore H_2O and the solution was filtered before adding 800 mL of methanol. The solution was stirred for 10 minutes in the ultrasound bath and degassed.

For the IND mobile phase preparation, 70 mL of acetic acid were added to 840 mL of Millipore H_2O and the solution was filtered before adding 1260 mL of Acetonitrile (ACN). The final solution was placed for 10 minutes in ultrasound bath.

4.2.6. HPLC

Isocratic reverse-phase HPLC was used for the determination of the TH and IND concentrations in the samples on a Shimadzu Prominence instrument from Shimadzu (Kyoto, Japan). The HPLC methods used for the model permeants are shown in table 5.

Table 5. The HPLC methods of the model permeants

	THEOPHYLLINE (TH)	**INDOMETHACIN (IND)**
Column type	LiChroCART 250-4, LiChrospher 100, RP-18,5 µm	LiChroCART 250-4, LiChrospher 100, RP-18,5 µm
Flow (mL/min)	1.2	2
Volume of injection (µL)	20	100
Mobile phase	MeOH/ NaH_2PO_4 *$2H_2O$ 4:6	ACN/H_2O/CH_3COOH 90:60:5 v/v
Wavelength (nm)	272	260
Run (min)	3.75	4
Temperature (°C)	35	40

4.3. Statistical analysis

ANOVA with Tukey or Dunnett's post was used to compare data. Only $P < 0.05$ values were considered of statistical significance during analysis with GraphPad Prism 8.2.1 (GraphPad Software, San Diego, California). All data are shown as means ± SD, with the number of replicates (n) is separately indicated in each figure.

5. Results and discussion

The aim of the present study was to identify the potential effect of the presence of different NMF components to the water uptake, microstructure and permeability of human skin isolated lipids. Four different NMF components were chosen for this study, concretely PCA, UCA, Urea, and Gly. The molecular structures of these compounds are given in Figure 11.

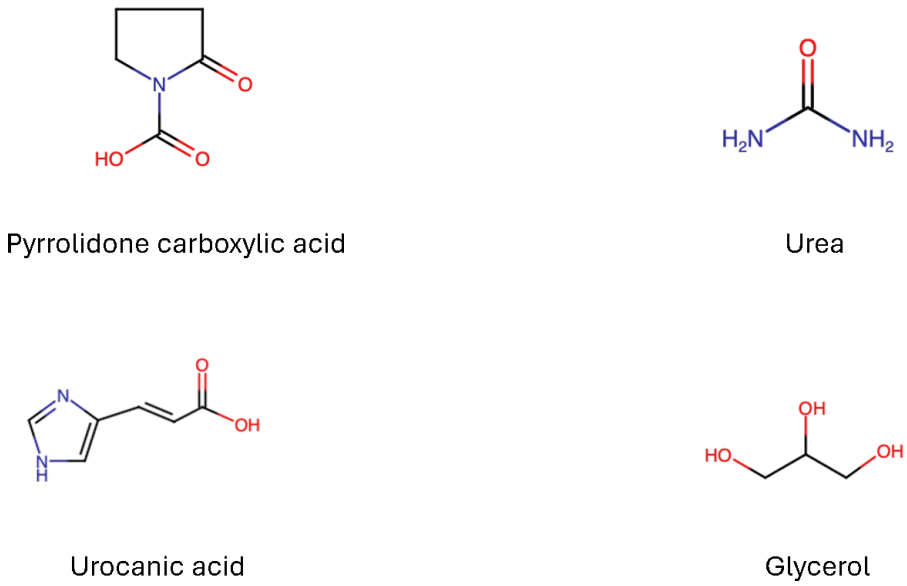

Figure 11. Chemical structures of PCA, UCA, Urea and Gly.

To determine the ideal conditions for detecting a possible effect, different molar ratios of the studied NMF components were chosen, keeping the lipid amount unchanged across all conditions. The preliminary NMF molar ratios consisted of 5%, 10%, and 50% over the total lipid content.

To fully incorporate lipids and NMF components in the same solution, which differ greatly from a solubility standpoint, it was necessary to identify a solvent or mixture of solvents capable of dissolving the investigated NMF while not affecting the solubility of the lipidic mixture. In this case, the mixture of hexane: EtOH 96% (2:1 v/v) identified as a convenient medium overcoming the obstacle, since EtOH 96% dissolves the polar part of lipids, while hexane is used to dissolve the non-polar part. At the same time, hexane: EtOH 96% (2:1 v/v) dissolved urea, whereas EtOH 96% proved to be an appropriate solvent for PCA, UCA and

Gly. Once the NMF stock solutions (1 mg/mL) were prepared, appropriate amounts were added to the lipidic mixture to create the model lipid membranes (Figure 11).

After spraying the selected lipid mixtures with or without the presence of NMF, an annealing step was performed to allow the lipids to organize in their desired lamellar and lateral structures. To understand if and how the presence of NMFs alone was affecting the lamellar and lateral structures of the lipidic mixtures, XRD, Confocal Raman microspectroscopy, and FTIR studies were performed.

XRD results of all tested samples are summarized in Figure 12. Organized lipid lamellae were observed for all samples by the formation of LPP (blue dotes) having length within physiological ranges (~13 nm). No significant differences were noticed at the LPP length between the control samples and the NMF containing samples in all tested concentrations. In some of the samples, not well resolved reflections which could be assigned to the formation of SPP were noticed (black dotes) but their absence from the majority of the tested samples suggested that they could be a potential artifact. On the other hand, reflections of separated Chol phase were visible (red dotes), consistent with a physiological repeated distance of ~3.4 nm for all the samples (except the 10% PCA) again without significant differences between the control and the NMF containing samples.

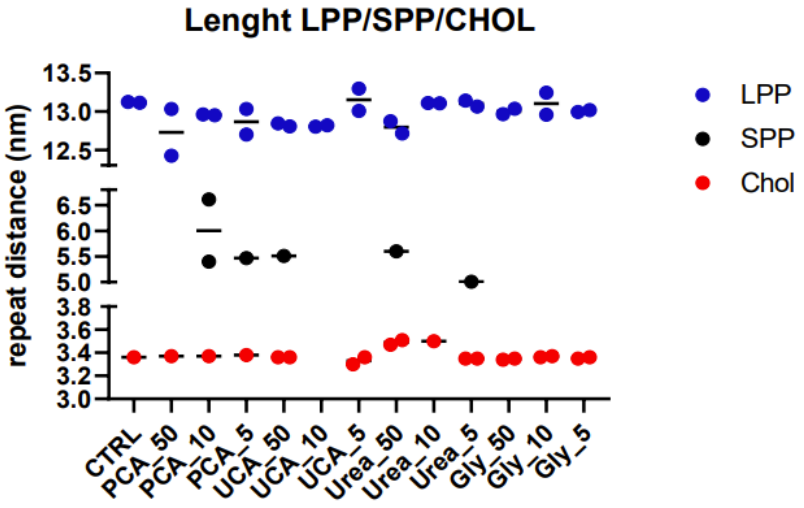

Figure 12. XRD evaluation of lamellar phases

Overall, XRD showed the expected lamellar organization within the lipids of the model membranes, indicating that the presence of different NMF molar ratios were mildly or not at all affecting the lamellar lipid organization.

Subsequently, confocal Raman microspectroscopy was carried out to determine a rough surface analysis of the model lipid membranes with the presence or the absence of different concentrations of NMF components. Representative images of selected samples are shown in Figure 13.

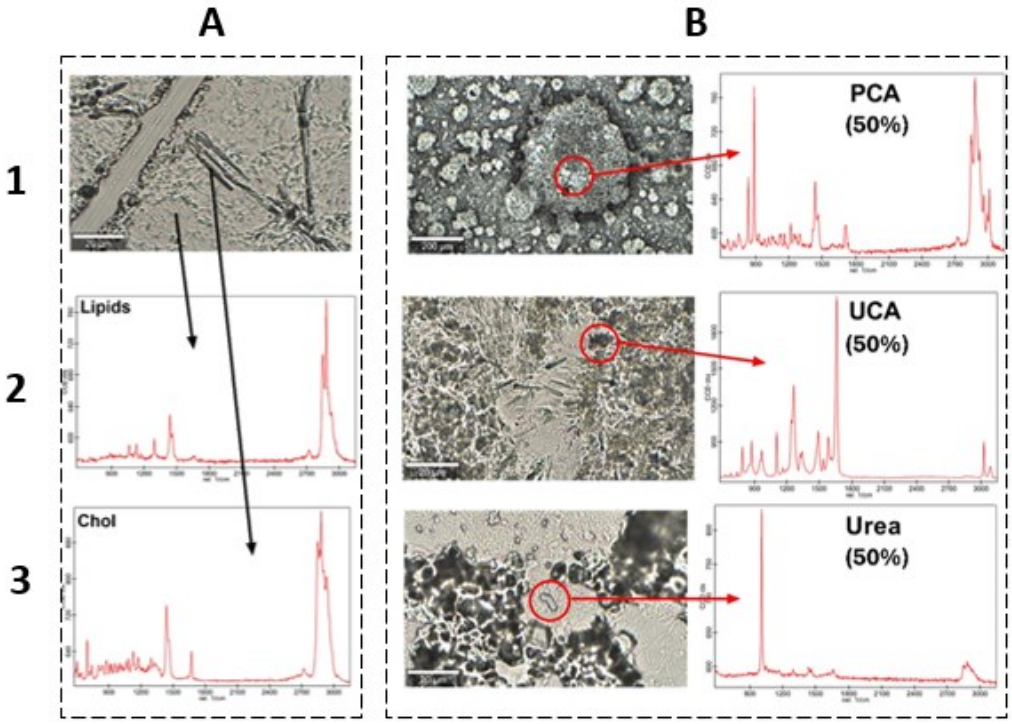

Figure 13. Raman spectroscopy evaluation

The control samples revealed predominantly homogenous areas (Panel A1) having the expected general lipid spectrum (Panel A2) together with areas assigned to separated crystalline Chol (Panel A3). For the NMF containing samples different characteristics were observed; Gly-containing samples of all tested concentrations and PCA-, UCA- and urea-containing samples of the lowest concentration (5%) exhibited a similar pattern to the control samples (not shown data). Interestingly, PCA and UCA containing samples at high molar concentrations (10% and 50%) showed clusters full of the NMF component (representative images of PCA and UCA containing samples at 50% are shown in Panels B1 and B2 respectively). In addition, urea-containing samples at high molar ratios (10% and 50%) revealed the presence of urea crystals (representative image of urea containing sample at 50% is shown in Panel B3). From these findings, it was revealed that the model lipid membranes with 10% and 50% of the NMF component were oversaturated since pure NMF spectra were detected. Thus, these ratios were excluded from further experiments and only the models containing 5% of the NMF component were used.

For the four NMF components (PCA, UCA, urea, and Gly) at 5% molar ratio, FTIR analysis was performed. FTIR data of lipid mixtures can give an insight of the lipid lateral packing by observing the CH2 symmetric vibration at around 2850 cm^{-1} and the intensity ratio of the CH2 rocking band doublet at 730 and 720 cm^{-1}. FTIR data of the lipid mixtures (Figure 14) showed well-organized lipids. An all-trans chain conformation is suggested by the CH2 symmetric stretching vibration values which were < 2850.0 cm^{-1}. In addition, a rocking band doublet at 730 to 720 cm^{-1} with a ratio of intensity ~ 0.5-0.6 indicated an orthorhombic chain packing. The absence of significant differences between the tested samples suggests that the presence of NMF components in low concentration (5%) is not affecting the lateral organization of the skin lipids.

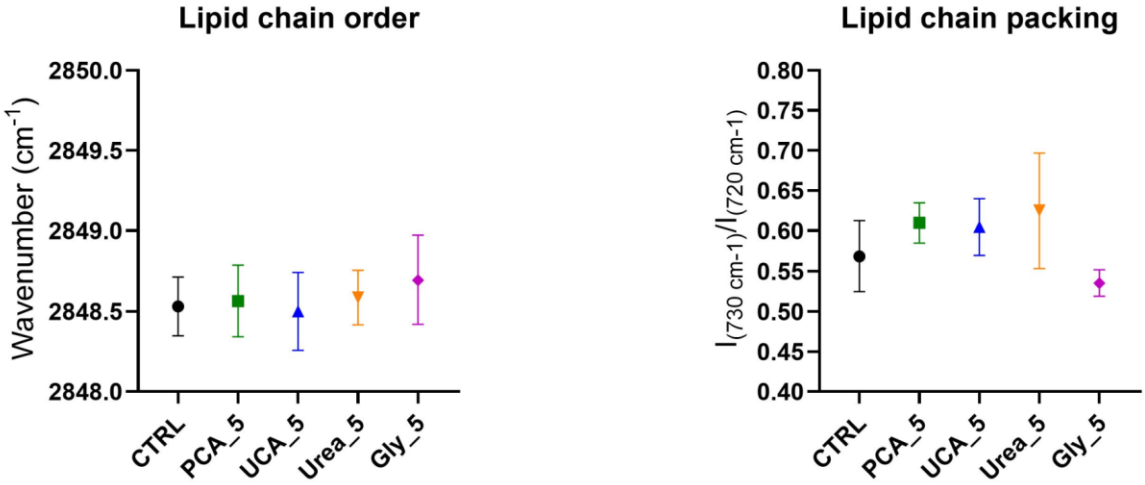

Figure 14.Evaluation of FTIR

After exploring the effect of the selected NMF components to the lamellar and lateral orientation of skin lipids, it was decided to determine whether the presence of the NMF components in the lipid mixture is affecting the amount of H_2O absorbed from the environment during the annealing process. This parameter was defined as H_2O loading and obtained immediately after the annealing phase (the mass of the glass supports was measured before and after the annealing process). At the same time, the evaluation of the H_2O retaining abilities of NMF were of interest, that's why it was decided to investigate if, how much, and how quickly the absorbed amount of H_2O was lost, defining this step as kinetics of dehydration.

The results showing the amount of H_2O absorbed from the environment by the tested lipid mixtures are summarized in Figure 15. UCA, urea and Gly containing lipids attracted comparable amount of H_2O during the annealing procedure in comparison with control samples (no significant differences were observed). On the other hand, PCA containing lipids were able to absorb nearly double the amount of H_2O vapor compared to control samples and the other NMF components.

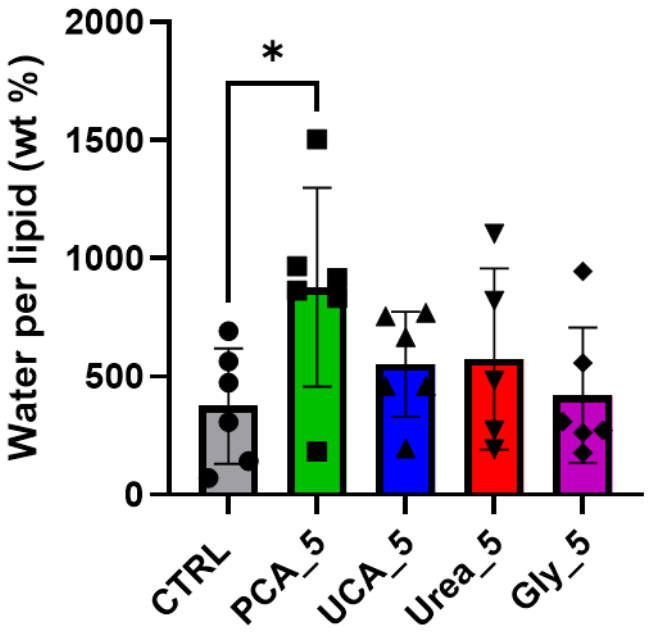

Figure 15. Water loading evaluation of 5% NMFs

It was expected that the presence of NMF would result in higher H_2O absorption in NMF-containing lipids. However, this was not observed in this experiment for UCA, urea, and Gly containing lipids. A possible explanation is that these NMF molecules are very tightly oriented and incorporated inside the lipid structure and between the lipid chains and their hydrophilic functional groups are not directly exposed to the outside environment in order to attract higher amounts of H_2O in comparison with the control samples. On the other hand, PCA containing lipids are absorbing more H_2O most probably because the PCA molecules, while mixed with the skin lipids, are oriented in a way that their hydrophilic part is more exposed to the environment making them able to absorb more H_2O in comparison with the control samples and the other NMF components.

Following the H_2O absorbance, the kinetics of dehydration were investigated over time by measuring the mass of the glass supports after the annealing process for a period of three hours. The results are presented as % of H_2O lost from each sample over time (Figure 16).

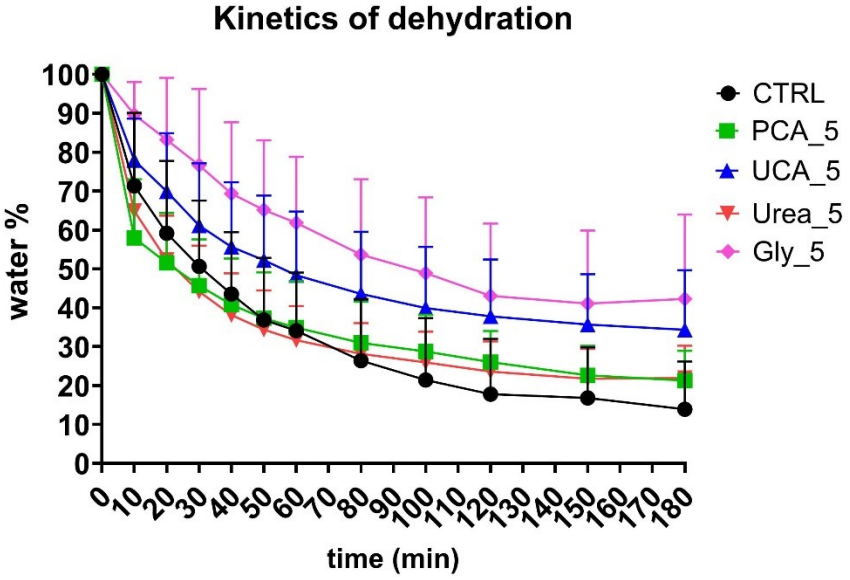

Figure 16. Kinetics of dehydration evaluation

It is not surprising that the control samples (black line) are quickly losing the absorbed amount of H_2O (50% of the absorbed H_2O amount is lost in the first 30 min and 90% of the absorbed H_2O is lost until the end of the experiment). A similar behavior was observed for the urea containing samples (red line) where 50% of the absorbed H_2O was lost in the first 20 min and 80% of the absorbed H_2O was lost until the end of the experiment. This finding suggests that the presence of urea molecules in the lipid mixture is not having any major effect neither to their hydration (proved earlier by the water loading) nor to their dehydration (proved by the kinetics of dehydration). What is interesting to observe is the fact that the PCA containing lipids (green line), even if they earlier proved to attract significantly higher amounts of H_2O molecules, they are unable to retain the absorbed H_2O and their dehydration profile is similar with the control and the urea samples (50% of the absorbed H_2O was lost in the first 20 min and 80% of the absorbed H_2O was lost until the end of the experiment). Of course, in absolute values the H_2O remaining in the lipids containing PCA after the end of the experiment is higher than the control or the urea containing samples (data not shown). The UCA containing samples (blue line) have the tendency to lose the absorbed H_2O with a slower rate (50% of the absorbed

H_2O was lost after 80 min) than the previous NMF components and 60% of the absorbed H_2O was lost at the end of the experiment. The best H_2O retaining NMF component (even without significant differences with the UCA containing samples) proved to be Gly (pink line) which is losing 50% of the absorbed H_2O after 100 min and is able to retain 40% of the absorbed water at the end of the experiment.

Overall, PCA and urea could be classified as the least efficient NMF-containing models since their H_2O retention abilities were comparable to the control samples at the end of the experiment. Interestingly, even though PCA was able to attract more H_2O than the other NMF, the H_2O retention was ineffective (quick loss). On the other hand, Gly and UCA demonstrated sufficient H_2O retaining abilities compared to the rest of the models and could be considered for further studies in a humidity-controlled setup to gather further information on their behavior once incorporated into human SC lipids. It is worth mentioning that, although Gly- and UCA-containing lipids absorbed the same amount of H_2O as the control samples, the NMF-containing samples were able to retain it more efficiently. Most probably, the presence of these NMF in the lipidic mixture is not responsible to absorb H_2O from the environment but is able to retain the existing H_2O molecules in the mixture.

In a further investigation, the four NMF components were sprayed on polycarbonate membranes at a molar ratio of 5% and the prepared membranes were tested for their barrier properties against 4 model permeants (H_2O, ions, TH, and IND).

During the permeation experiments (Figure 17), TEWL data showed unusually high values. More specifically, the control membranes had an unusually high H_2O loss of 43.52 ± 20.98 ($g/m^2/h$), compared to the normal values (~10- 20 $g/m^2/h$) [94, 95]. No significant differences of the TEWL values were observed between NMF containing membranes and the control samples. The control values of EI were 212.89 ± 168.89 ($k\Omega \times cm^2$), without significant differences between them and the NMF containing samples.

The flux of TH through the control membranes was 0.59 ± 0 24 ($\mu g/cm^2/h$), which is unexpectedly higher when compared to previous experiments with similar control membranes (previous observed values were ~ 0.1 $\mu g/cm^2/h$). There were again no significant differences between NMF containing membranes and the control membranes. The IND flux through the control membranes was 1.02 ± 0.2 $\mu g/cm^2/h$. Again, this value is much higher than the values observed during previous experiments with similar control membranes [94-96].

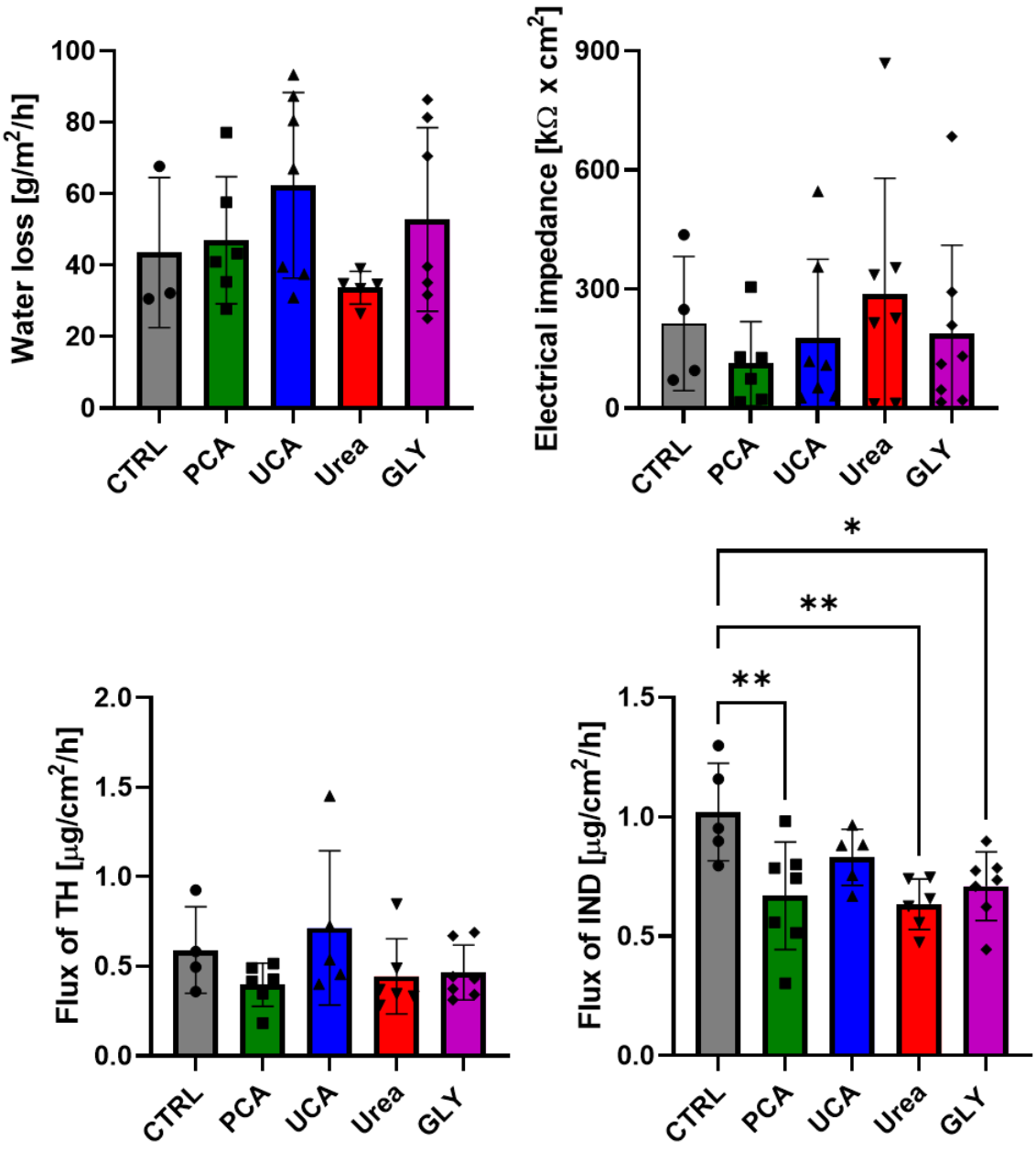

Figure 17. Permeation experiment (TEWL, EI), TH&IND flux.

In general, the majority of the permeability testing of the membranes (TEWL, EI and TH) revealed no differences between control and NMF-containing membranes. Besides that, the control values for TEWL and the flux of model permeants were unusually high when compared to previous studies using the same controls. From the obtained data it was assumed that there was most probably a mistake in the setup, and the experiment should be repeated.

6.Conclusion

The aim of this study was to investigate the potential impact of NMF components on the microstructure, H_2O absorption, H_2O retainment, and permeability of lipids in model lipid membranes.

XRD demonstrated the expected organization within the lipids of the model membranes, indicating that the presence or different molar ratios of NMF (5%, 10% and 50%) had no effect on the lamellar lipid organization. Raman spectroscopy demonstrated that high concentration of NMF (10% and 50%) resulted in non-homogeneous mixtures with visible clusters and crystals, whereas 5% resulted in more homogeneous mixtures proving better incorporation of the NMF in the lipids. FTIR studies provided information on orthorhombic lateral packing, but no significant differences were found between NMF containing samples and control samples. The H_2O loading experiment demonstrated that the H_2O absorbance for NMF containing lipids was not significantly higher than the control, except for PCA, most likely due to a different orientation of NMF molecules within the lipidic mixture. Interestingly, in the kinetic dehydration experiment, Gly and UCA-containing lipids lost the absorbed H_2O at a slower rate. The permeation experiment resulted in unusually high permeation values of permeants for control samples, and they were not further evaluated.

Overall, the obtained findings were used as preliminary data for further experiments with Gly and UCA containing lipid mixtures in a 5% ratio.

1. Kanitakis, J., *Anatomy, histology and immunohistochemistry of normal human skin.* Eur J Dermatol, 2002. **12**(4): p. 390-9; quiz 400-1.
2. Rawlings, A.V. and C.R. Harding, *Moisturization and skin barrier function.* Dermatol Ther, 2004. **17 Suppl 1**: p. 43-8.
3. Czekalla, C., et al., *Noninvasive Determination of Epidermal and Stratum Corneum Thickness in vivo Using Two-Photon Microscopy and Optical Coherence Tomography: Impact of Body Area, Age, and Gender.* Skin Pharmacol Physiol, 2019. **32**(3): p. 142-150.
4. Elias, P.M. and G.K. Menon, *Structural and lipid biochemical correlates of the epidermal permeability barrier.* Adv Lipid Res, 1991. **24**: p. 1-26.
5. Chan, Y.H. and S.G. Boxer, *Model membrane systems and their applications.* Curr Opin Chem Biol, 2007. **11**(6): p. 581-7.
6. Escribá, P.V., et al., *Membranes: a meeting point for lipids, proteins and therapies.* J Cell Mol Med, 2008. **12**(3): p. 829-75.
7. Casares, D., P.V. Escribá, and C.A. Rosselló, *Membrane Lipid Composition: Effect on Membrane and Organelle Structure, Function and Compartmentalization and Therapeutic Avenues.* Int J Mol Sci, 2019. **20**(9).
8. Mescher, A.L., *Skin*, in *Junqueira's Basic Histology Text and Atlas, 16e*. 2021, McGraw Hill: New York, NY.
9. Oliver, G. and K. Alitalo, *The lymphatic vasculature: recent progress and paradigms.* Annu Rev Cell Dev Biol, 2005. **21**: p. 457-83.
10. Paquet-Fifield, S., et al., *Vascular Endothelial Growth Factor-d Modulates Caliber and Function of Initial Lymphatics in the Dermis.* Journal of Investigative Dermatology, 2013. **133**(8): p. 2074-2084.
11. Achen, M.G., G.B. Mann, and S.A. Stacker, *Targeting lymphangiogenesis to prevent tumour metastasis.* Br J Cancer, 2006. **94**(10): p. 1355-60.
12. Cueni, L.N. and M. Detmar, *The lymphatic system in health and disease.* Lymphat Res Biol, 2008. **6**(3-4): p. 109-22.
13. Alitalo, K., *The lymphatic vasculature in disease.* Nat Med, 2011. **17**(11): p. 1371-80.
14. Baldwin, M.E., S.A. Stacker, and M.G. Achen, *Molecular control of lymphangiogenesis.* Bioessays, 2002. **24**(11): p. 1030-40.
15. Rippa, A.L., E.P. Kalabusheva, and E.A. Vorotelyak, *Regeneration of Dermis: Scarring and Cells Involved.* Cells, 2019. **8**(6).
16. Anselmo, A.C., Y. Gokarn, and S. Mitragotri, *Non-invasive delivery strategies for biologics.* Nature Reviews Drug Discovery, 2019. **18**(1): p. 19-40.
17. Newell, B.B. and W. Zhan, *Numerical simulation of transdermal delivery of drug nanocarriers using solid microneedles and medicated adhesive patch.* International Journal of Heat and Mass Transfer, 2024. **223**: p. 125291.
18. Baroni, A., et al., *Structure and function of the epidermis related to barrier properties.* Clinics in Dermatology, 2012. **30**(3): p. 257-262.
19. Yousef, H., M. Alhajj, and S. Sharma, *Anatomy, skin (integument), epidermis.* 2017.
20. Murphrey, M.B., J.H. Miao, and P.M. Zito, *Histology, stratum corneum.* 2018.
21. Scheuplein, R.J. and I.H. Blank, *Permeability of the skin.* Physiol Rev, 1971. **51**(4): p. 702-47.
22. Del Rosso, J.Q. and J. Levin, *The clinical relevance of maintaining the functional integrity of the stratum corneum in both healthy and disease-affected skin.* J Clin Aesthet Dermatol, 2011. **4**(9): p. 22-42.
23. Proksch, E., J.-m. Jensen, and P.M. Elias, *Skin lipids and epidermal differentiation in atopic dermatitis.* Clinics in dermatology, 2003. **21**(2): p. 134-144.
24. Leyden, J.J. and A.V. Rawlings, *Skin moisturization*. 2002: CRC Press.
25. Harding, C.R., *The stratum corneum: structure and function in health and disease.* Dermatologic therapy, 2004. **17**: p. 6-15.
26. Elias, P., *Cosmeceuticals.* 2005.

27. Beddoes, C.M., G.S. Gooris, and J.A. Bouwstra, *Preferential arrangement of lipids in the long-periodicity phase of a stratum corneum matrix model.* J Lipid Res, 2018. **59**(12): p. 2329-2338.
28. Bouwstra, J., G. Gooris, and M. Ponec, *The lipid organisation of the skin barrier: liquid and crystalline domains coexist in lamellar phases.* J Biol Phys, 2002. **28**(2): p. 211-23.
29. Bouwstra, J.A., et al., *Structural investigations of human stratum corneum by small-angle X-ray scattering.* J Invest Dermatol, 1991. **97**(6): p. 1005-12.
30. de Jager, M.W., M. Ponec, and J.A. Bouwstra, *11 The Lipid Organization in Stratum Corneum and Model Systems Based on Ceramides.* Enhancement in drug delivery, 2007.
31. White, S.H., D. Mirejovsky, and G.I. King, *Structure of lamellar lipid domains and corneocyte envelopes of murine stratum corneum. An X-ray diffraction study.* Biochemistry, 1988. **27**(10): p. 3725-3732.
32. Bouwstra, J., et al., *The lipid organisation in the skin barrier.* Acta dermato-venereologica, 2000. **80**.
33. Hatta, I., et al., *Coexistence of two domains in intercellular lipid matrix of stratum corneum.* Biochimica et Biophysica Acta (BBA)-Biomembranes, 2006. **1758**(11): p. 1830-1836.
34. Groen, D., et al., *Is an orthorhombic lateral packing and a proper lamellar organization important for the skin barrier function?* Biochimica et Biophysica Acta (BBA) - Biomembranes, 2011. **1808**(6): p. 1529-1537.
35. Janssens, M., et al., *Increase in short-chain ceramides correlates with an altered lipid organization and decreased barrier function in atopic eczema patients.* Journal of lipid research, 2012. **53**.
36. Mojumdar, E., et al., *Stratum corneum lipid matrix: Location of acyl ceramide and cholesterol in the unit cell of the long periodicity phase.* Biochimica et Biophysica Acta (BBA)-Biomembranes, 2016. **1858**(8): p. 1926-1934.
37. Fandrei, F., et al., *The intriguing molecular dynamics of Cer[EOS] in rigid skin barrier lipid layers requires improvement of the model.* Journal of Lipid Research, 2023. **64**(5): p. 100356.
38. Bouwstra, J.A., et al., *Role of ceramide 1 in the molecular organization of the stratum corneum lipids.* Journal of lipid research, 1998. **39**(1): p. 186-196.
39. Mojumdar, E., G. Gooris, and J. Bouwstra, *Phase behavior of skin lipid mixtures: the effect of cholesterol on lipid organization.* Soft matter, 2015. **11**(21): p. 4326-4336.
40. Van Smeden, J., et al., *The important role of stratum corneum lipids for the cutaneous barrier function.* Biochimica et Biophysica Acta (BBA)-Molecular and Cell Biology of Lipids, 2014. **1841**(3): p. 295-313.
41. Motta, S., et al., *Ceramide composition of the psoriatic scale.* Biochimica et Biophysica Acta (BBA)-Molecular Basis of Disease, 1993. **1182**(2): p. 147-151.
42. Descamps, F., et al., *Lamellar lipid organization and ceramide composition in the stratum corneum of patients with atopic eczema.* J Eur Acad Dermatol Venereol, 2011. **18**: p. 13-26.
43. Sahle, F.F., et al., *Skin diseases associated with the depletion of stratum corneum lipids and stratum corneum lipid substitution therapy.* Skin pharmacology and physiology, 2015. **28**(1): p. 42-55.
44. Vávrová, K., A. Kováčik, and L. Opálka, *Ceramides in the skin barrier.* Acta Facultatis Pharmaceuticae Universitatis Comenianae, 2017. **64**.
45. van Smeden, J., et al., *Skin barrier lipid enzyme activity in Netherton patients is associated with protease activity and ceramide abnormalities [S].* Journal of lipid research, 2020. **61**(6): p. 859-869.
46. Rawlings, A.V. and P.J. Matts, *Stratum corneum moisturization at the molecular level: an update in relation to the dry skin cycle.* J Invest Dermatol, 2005. **124**(6): p. 1099-110.
47. Gunnarsson, M., et al., *Extraction of natural moisturizing factor from the stratum corneum and its implication on skin molecular mobility.* J Colloid Interface Sci, 2021. **604**: p. 480-491.

48. Harding, C.R., et al., *Dry skin, moisturization and corneodesmolysis.* Int J Cosmet Sci, 2000. **22**(1): p. 21-52.
49. Clar, E.J. and A. Fourtanier, *Pyrrolidone carboxylic acid and the skin.* Int J Cosmet Sci, 1981. **3**(3): p. 101-13.
50. Kezic, S., et al., *Levels of filaggrin degradation products are influenced by both filaggrin genotype and atopic dermatitis severity.* Allergy, 2011. **66**(7): p. 934-40.
51. Ishida-Yamamoto, A. and H. Iizuka, *Structural organization of cornified cell envelopes and alterations in inherited skin disorders.* Exp Dermatol, 1998. **7**(1): p. 1-10.
52. Rawlings, A.V., et al., *Stratum corneum moisturization at the molecular level.* J Invest Dermatol, 1994. **103**(5): p. 731-41.
53. Barrett, J.G. and I.R. Scott, *Pyrrolidone carboxylic acid synthesis in guinea pig epidermis.* J Invest Dermatol, 1983. **81**(2): p. 122-4.
54. Harding, C.R. and I.R. Scott, *Histidine-rich proteins (filaggrins): structural and functional heterogeneity during epidermal differentiation.* J Mol Biol, 1983. **170**(3): p. 651-73.
55. Björklund, S., et al., *Stratum corneum molecular mobility in the presence of natural moisturizers.* Soft Matter, 2014. **10**(25): p. 4535-46.
56. Kezic, S., et al., *Natural moisturizing factor components in the stratum corneum as biomarkers of filaggrin genotype: evaluation of minimally invasive methods.* Br J Dermatol, 2009. **161**(5): p. 1098-104.
57. Pham, D.L., et al., *Increased cis-to-trans urocanic acid ratio in the skin of chronic spontaneous urticaria patients.* Sci Rep, 2017. **7**(1): p. 1318.
58. Abd, E., et al., *Skin models for the testing of transdermal drugs.* Clin Pharmacol, 2016. **8**: p. 163-176.
59. Bronaugh, R.L., R.F. Stewart, and E.R. Congdon, *Methods for in vitro percutaneous absorption studies II. Animal models for human skin.* Toxicology and applied pharmacology, 1982. **62**(3): p. 481-488.
60. Bronaugh, R.L., et al., *Determination of percutaneous absorption by in vitro techniques.* Drugs and the pharmaceutical sciences, 1999. **97**: p. 229-234.
61. Panchagnula, R., K. Stemmer, and W. Ritschel, *Animal models for transdermal drug delivery.* Methods and findings in experimental and clinical pharmacology, 1997. **19**(5): p. 335-341.
62. Sato, K., K. Sugibayashi, and Y. Morimoto, *Species differences in percutaneous absorption of nicorandil.* Journal of pharmaceutical sciences, 1991. **80**(2): p. 104-107.
63. Schmook, F.P., J.G. Meingassner, and A. Billich, *Comparison of human skin or epidermis models with human and animal skin in in-vitro percutaneous absorption.* International journal of pharmaceutics, 2001. **215**(1-2): p. 51-56.
64. Vecchia, B.E. and A. Bunge, *Animal models: a comparison of permeability coefficients for excised skin from humans and animals.* Dermal absorption models in toxicology and pharmacology, 2006: p. 305-333.
65. Vallet, V., et al., *Percutaneous penetration and distribution of VX using in vitro pig or human excised skin: Validation of demeton-S-methyl as adequate simulant for VX skin permeation investigations.* Toxicology, 2008. **246**(1): p. 73-82.
66. Roberts, M.E. and K.R. Mueller, *Comparisons of in vitro nitroglycerin (TNG) flux across Yucatan pig, hairless mouse, and human skins.* Pharmaceutical Research, 1990. **7**(6): p. 673-676.
67. Barbero, A.M. and H.F. Frasch, *Pig and guinea pig skin as surrogates for human in vitro penetration studies: A quantitative review.* Toxicology in Vitro, 2009. **23**(1): p. 1-13.
68. Waters, J.L., *Recent Developments in Skin Mimic Systems to Predict Transdermal Permeation.* Current Pharmaceutical Design, 2015. **21**(20): p. 2725-2732.
69. Sinkó, B., et al., *A PAMPA study of the permeability-enhancing effect of new ceramide analogues.* Chemistry & biodiversity, 2009. **6**(11): p. 1867-1874.

70. Sinkó, B., et al., *Skin–PAMPA: A new method for fast prediction of skin penetration.* European Journal of Pharmaceutical Sciences, 2012. **45**(5): p. 698-707.
71. Engesland, A., et al., *New applications of phospholipid vesicle-based permeation assay: permeation model mimicking skin barrier.* Journal of Pharmaceutical Sciences, 2013. **102**(5): p. 1588-1600.
72. Engesland, A., N. Škalko-Basnet, and G.E. Flaten, *Phospholipid vesicle-based permeation assay and EpiSkin® in assessment of drug therapies destined for skin administration.* Journal of Pharmaceutical Sciences, 2015. **104**(3): p. 1119-1127.
73. de Jager, M., et al., *A novel in vitro percutaneous penetration model: evaluation of barrier properties with p-aminobenzoic acid and two of its derivatives.* Pharmaceutical research, 2006. **23**: p. 951-960.
74. Ochalek, M., et al., *SC lipid model membranes designed for studying impact of ceramide species on drug diffusion and permeation–Part II: Diffusion and permeation of model drugs.* European journal of pharmaceutics and biopharmaceutics, 2012. **82**(2): p. 360-366.
75. Zhang, C., et al., *High performance affinity chromatography and related separation methods for the analysis of biological and pharmaceutical agents.* Analyst, 2018. **143**(2): p. 374-391.
76. Snyder, L.R., J.J. Kirkland, and J.L. Glajch. *Practical HPLC method development*. 1988.
77. Moldoveanu, S.C. and V. David, *Chapter 4 - Basic Information Regarding the HPLC Techniques*, in *Selection of the HPLC Method in Chemical Analysis*, S.C. Moldoveanu and V. David, Editors. 2017, Elsevier: Boston. p. 87-187.
78. Ahuja, S., *Handbook of pharmaceutical analysis by HPLC* 2005, Amsterdam Elsevier Academic Press.
79. Skoog, D.A., F.J. Holler, and S.R. Crouch, *Principles of Instrumental Analysis*. 2017: Cengage Learning.
80. Rusli, H., R.M. Putri, and A. Alni, *Recent Developments of Liquid Chromatography Stationary Phases for Compound Separation: From Proteins to Small Organic Compounds.* Molecules, 2022. **27**(3).
81. Egawa, M., *Raman microscopy for skin evaluation.* Analyst, 2021. **146**(4): p. 1142-1150.
82. Das, R.S. and Y.K. Agrawal, *Raman spectroscopy: Recent advancements, techniques and applications.* Vibrational Spectroscopy, 2011. **57**(2): p. 163-176.
83. Rebrosova, K., et al., *Raman Spectroscopy-A Novel Method for Identification and Characterization of Microbes on a Single-Cell Level in Clinical Settings.* Front Cell Infect Microbiol, 2022. **12**: p. 866463.
84. Lunter, D., et al., *Novel aspects of Raman spectroscopy in skin research.* Exp Dermatol, 2022. **31**(9): p. 1311-1329.
85. Akdeniz, M., et al., *Transepidermal water loss in healthy adults: a systematic review and meta-analysis update.* Br J Dermatol, 2018. **179**(5): p. 1049-1055.
86. Klotz, T., et al., *Devices measuring transepidermal water loss: A systematic review of measurement properties.* Skin Res Technol, 2022. **28**(4): p. 497-539.
87. Berardesca, E., et al., *The revised EEMCO guidance for the in vivo measurement of water in the skin.* Skin Res Technol, 2018. **24**(3): p. 351-358.
88. du Plessis, J., et al., *International guidelines for the in vivo assessment of skin properties in non-clinical settings: Part 2. transepidermal water loss and skin hydration.* Skin Res Technol, 2013. **19**(3): p. 265-78.
89. Alexander, H., et al., *Research Techniques Made Simple: Transepidermal Water Loss Measurement as a Research Tool.* J Invest Dermatol, 2018. **138**(11): p. 2295-2300.e1.
90. Green, M., et al., *Transepidermal water loss (TEWL): Environment and pollution-A systematic review.* Skin Health Dis, 2022. **2**(2): p. e104.
91. Alexander, H., et al., *Research Techniques Made Simple: Transepidermal Water Loss Measurement as a Research Tool.* Journal of Investigative Dermatology, 2018. **138**: p. 2295-2300.e1.

92. Fasano, W. and P. Hinderliter, *The Tinsley LCR Databridge Model 6401 and electrical impedance measurements to evaluate skin integrity in vitro.* Toxicology in vitro, 2004. **18**(5): p. 725-729.
93. White, E.A., M.E. Orazem, and A.L. Bunge, *A critical analysis of single-frequency LCR databridge impedance measurements of human skin.* Toxicology in Vitro, 2011. **25**(4): p. 774-784.
94. Sochorová, M., et al., *Permeability and microstructure of cholesterol-depleted skin lipid membranes and human stratum corneum.* Journal of Colloid and Interface Science, 2019. **535**: p. 227-238.
95. Fandrei, F., et al., *Cholesterol sulfate fluidizes the sterol fraction of the stratum corneum lipid phase and increases its permeability.* J Lipid Res, 2022. **63**(3): p. 100177.
96. Sochorová, M., et al., *Permeability Barrier and Microstructure of Skin Lipid Membrane Models of Impaired Glucosylceramide Processing.* Sci Rep, 2017. **7**(1): p. 6470.